

# A New Formulation Of Lee-Wick Quantum Field Theory

*Damiano Anselmi<sup>1</sup> and Marco Piva<sup>2</sup>*

*Dipartimento di Fisica “Enrico Fermi”, Università di Pisa,*

*Largo B. Pontecorvo 3, 56127 Pisa, Italy*

*and INFN, Sezione di Pisa,*

*Largo B. Pontecorvo 3, 56127 Pisa, Italy*

## Abstract

The Lee-Wick models are higher-derivative theories that are claimed to be unitary thanks to a peculiar cancelation mechanism. In this paper, we provide a new formulation of the models, to clarify several aspects that have remained quite mysterious, so far. Specifically, we define them as nonanalytically Wick rotated Euclidean theories. The complex energy plane is divided into disconnected regions, which can be related to one another by keeping the integration domain on the space momenta rigid when certain poles cross it. Working in a generic Lorentz frame, the models are intrinsically equipped with the right recipe to treat the pinchings of the Lee-Wick poles, with no need of external *ad hoc* prescriptions. We describe these features in detail by calculating the one-loop bubble diagram and explaining how the key properties generalize to more complicated diagrams. The physical results of our formulation are different from those of the previous ones. The unusual behaviors of the physical amplitudes lead to interesting phenomenological predictions.

---

<sup>1</sup>damiano.anselmi@unipi.it

<sup>2</sup>marco.piva@df.unipi.it

# 1 Introduction

The Lee-Wick (LW) models are special higher-derivative theories, defined in a peculiar way, which are claimed to lead to a perturbatively unitary  $S$  matrix [1, 2, 3]. Precisely, the claim is that they are equipped with well defined cutting equations, such that if we project the initial and final states onto the subspace  $V$  of physical degrees of freedom, only states belonging to the same space  $V$  propagate through the cuts. Several properties of the models and aspects of their formulation have not been clarified exhaustively, so far. In this paper we plan to overcome those problems by reformulating the theories completely. We also show that our formulation gives physical predictions that differ from those of the previous ones.

It is well known that higher-derivative kinetic Lagrangian terms may improve the ultraviolet behaviors of the Feynman diagrams and may turn nonrenormalizable theories into renormalizable ones, as in the case of higher-derivative gravity [4]. However, the higher-derivative corrections, if not treated properly, lead to violations of unitarity or even mathematical inconsistencies [5]. The Lee-Wick idea is promising, because it claims to reconcile renormalizability and unitarity.

The propagators of the LW models contain extra poles, which we call *LW poles*, in addition to the poles corresponding to the physical degrees of freedom and the poles corresponding to the gauge degrees of freedom (such as the longitudinal and temporal components of the gauge fields and the poles of the Faddeev-Popov ghosts). The LW poles come in complex conjugate pairs, which we call *LW pairs*. Cutkosky *et al.* (CLOP) showed in ref. [3] that the  $S$  matrix is not analytic when pairs of LW poles pinch. Analyticity is a property we are accustomed to, but not a fundamental physical requirement. Nakanishi [6] showed that, if defined in a certain way, the models violate Lorentz invariance. This problem is more serious, but it can be avoided by defining the theories in a different way. In ref. [3] it was proposed to treat the pinching of the LW poles by means of a procedure of limit, which is known as *CLOP prescription*. In simple diagrams, the CLOP prescription gives an unambiguous and unitary result, as confirmed by the calculations of Grinstein *et al.* [7] in the case of the bubble diagram. However, it is not clear how to incorporate the CLOP prescription into a Lagrangian and ambiguities are expected in high-order diagrams [3]. This leads us to claim that some key issues concerning the formulation of the LW models have remained open and are awaiting to be clarified.

It is more convenient to completely change approach and define the LW models as nonanalytically Wick rotated Euclidean higher-derivative theories. First, we know from ref. [5] that a Minkowski formulation of such a type of higher-derivative theories is not

viable, since in general it generates nonlocal, non-Hermitian divergences that cannot be removed by any standard approach. The Wick rotation from the Euclidean framework is thus expected to play a crucial role, because it is the only viable path.

However, the Wick rotation of the higher-derivative theories we are considering turns out to be nonanalytic, because of the LW pinching, to the extent that the complex energy plane is divided into disjoint regions. The Lorentz violation is avoided by working in a generic Lorentz frame and with generic external momenta and then analytically continuing in each region separately. We show that, if we do so, the models are intrinsically equipped with all that is necessary to define them properly. In particular, there is no need of the CLOP prescription, or any other prescription to handle the pinching of the LW poles. Actually, the CLOP prescription should be dropped, because it leads to physical results that differ from those of our formulation, even in a simple case such as the bubble diagram with different masses.

The behaviors of the amplitudes show some unexpected features, which lead to interesting phenomenological predictions. In particular, the violation of analyticity is quite apparent, when the amplitude is plotted. If ever observed, this behavior could be the quickest way to determine the experimental value of the energy scale  $M$  associated with the higher-derivative terms, which is the key physical constant of the LW models.

The Lee-Wick models have been also explored for their possible physical applications, which include QED [2], the standard model [8], grand unified theories [9] and quantum gravity [10].

The paper is organized as follows. In section 2, we outline the formulation of the LW models as nonanalytically Wick rotated Euclidean theories. In section 3 we study the LW pinching in detail, in the case of the bubble diagram. In section 4, we describe the calculations of the physical amplitudes in a neighborhood of the LW pinching and show that the CLOP and similar prescriptions are not consistent with our approach. In section 5 we evaluate the bubble diagram in the new formulation and show that the physical results are in general different from those that follow from the CLOP and other prescriptions. We also comment on the phenomenological relevance of the results. In section 6 we explain how to deal with more complicated diagrams.

## 2 Lee-Wick models as Wick rotated Euclidean theories

In this section we outline the new formulation of the LW models. We begin by describing the class of higher-derivative theories that we are considering. The higher-derivative Lagrangian terms are multiplied by inverse powers of certain mass scales, which we call  $LW$

scales. For simplicity, we can assume that there is just one LW scale, which we denote by  $M$ , since the generalization to many LW scales is straightforward.

When  $M$  tends to infinity, the propagators must tend to the ones of ordinary unitary theories. Moreover, the extra poles that are present when  $M < \infty$  must have nontrivial real and imaginary parts and come in complex conjugate pairs.

A typical propagator of momentum  $p$  is equal to the standard propagator times a real function of  $p^2$  that has no poles on the real axis. For concreteness, we take

$$iD(p^2, m^2, \epsilon) = \frac{iM^4}{(p^2 - m^2 + i\epsilon)((p^2)^2 + M^4)}. \quad (2.1)$$

More general propagators can be considered. In particular renormalization may lead to structures such as

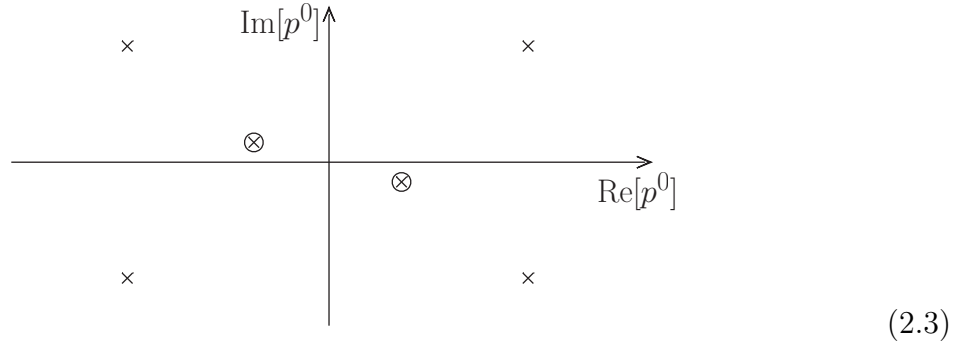
$$\frac{iM^4}{(p^2 - m^2 + i\epsilon)((p^2 - \mu^2)^2 + M^4)}.$$

However, the key features are already encoded in (2.1) and the extension does not change the sense of our investigation.

The poles of (2.1) are

$$p^0 = \pm\omega_m(\mathbf{p}) \mp i\epsilon, \quad p^0 = \pm\omega_M(\mathbf{p}), \quad p^0 = \pm\omega_M^*(\mathbf{p}), \quad (2.2)$$

where  $\omega_m(\mathbf{p}) = \sqrt{\mathbf{p}^2 + m^2}$  and  $\omega_M(\mathbf{p}) = \sqrt{\mathbf{p}^2 + iM^2}$ . Their locations are shown in the picture



where the LW poles are denoted by means of an  $\times$ , while the standard poles are denoted by a circled  $\times$ .

We can integrate  $p^0$  along the real axis or along the imaginary axis. The first choice defines the Minkowski theory, the second choice defines the Euclidean theory. The two give different results, because, even if the integration path at infinity does not contribute, some poles are located in the first and third quadrants of the complex plane. In ref. [5] it was shown that in general the Minkowski theories of this type are inconsistent, because they are

plagued with nonlocal, non-Hermitian divergences that cannot be subtracted away. The bubble diagram in four dimensions is one of the few convergent exceptions, but it becomes nonlocally divergent as soon as nontrivial numerators are brought by the vertices, which happens for example in higher-derivative gravity. This fact forces us to proceed with the Euclidean theory.

Usually, the Wick rotation is an analytic operation, but in the Lee-Wick models the situation is different. The analytically Wick rotated Euclidean theory gives the Lee-Wick theory only in a region of the complex energy plane. It is the region that contains the imaginary axis, which we call *main region*. The complex plane turns out to be divided into several disconnected regions  $\mathcal{A}_i$ , which can be reached from the main region in a nonanalytic way. The regions  $\mathcal{A}_i$  are called *analytic regions*.

In the light of this fact, the calculation of the correlation functions proceeds as follows. The loop integrals are evaluated at generic (possibly complex) external momenta, in each analytic region  $\mathcal{A}_i$  of the complex plane. For a reason that we will explain, we anticipate that it is also necessary to work in a sufficiently generic Lorentz frame, because special Lorentz frames may squeeze an entire region  $\mathcal{A}_i$  to a branch cut. The  $\mathcal{A}_i$  subdomain where the calculation is done is denoted by  $\mathcal{O}_i$  and has to satisfy suitable properties. For example, it must contain an accumulation point.

After the evaluation, the amplitude is analytically continued from  $\mathcal{O}_i$  to the rest of the region  $\mathcal{A}_i$ . This procedure gives the amplitude of the LW model, region by region. Since it is not possible to relate the regions analytically, the Wick rotation is nonanalytic. Yet, the regions are related by a well-defined computational procedure, which we describe in the next sections.

We may condense their articulated definition by saying that *the LW models are non-analytically Wick rotated Euclidean higher-derivative theories of a special class*.

Consider the propagator (2.1) and its poles (2.2). When the imaginary axis is rotated to the real one, we get the integration path

(2.4)

The Wick rotation is less trivial when performed in Feynman diagrams. To be explicit, consider the bubble diagram


(2.5)

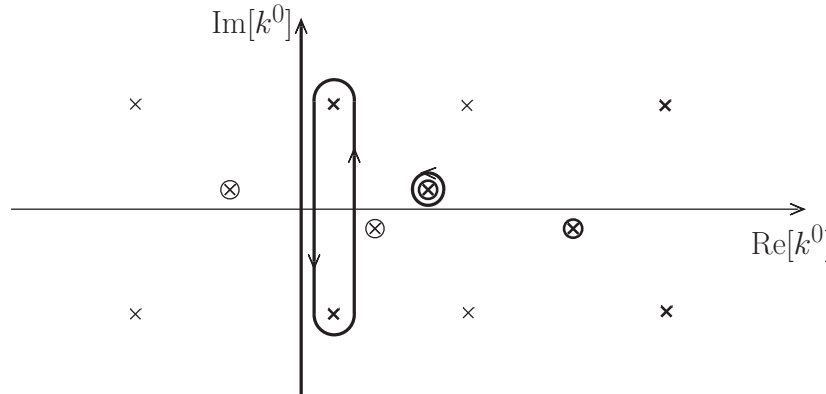
The bubble diagram has two propagators, so the number of poles doubles. If one propagator has momentum  $k$  and the other propagator has momentum  $k - p$ , we have a loop integral proportional to

$$\mathcal{J}(p) = \int \frac{d^D k}{(2\pi)^D} D(k^2, m_1^2, \epsilon_1) D((k - p)^2, m_2^2, \epsilon_2), \quad (2.6)$$

where  $D$  is the spacetime dimension. When we vary the external momentum  $p$ , the poles of the first propagator are fixed [given by formula (2.2) with  $p \rightarrow k$ ,  $m \rightarrow m_1$ ], while those of the second propagator, which are

$$k^0 = p^0 \pm \omega_{m_2}(\mathbf{k} - \mathbf{p}) \mp i\epsilon, \quad k^0 = p^0 \pm \omega_M(\mathbf{k} - \mathbf{p}), \quad k^0 = p^0 \pm \omega_M^*(\mathbf{k} - \mathbf{p}), \quad (2.7)$$

move on the complex plane. With respect to the fixed poles, this sextet of poles is translated by  $p^0$  and deformed by  $\mathbf{p}$ . At some point, the translation makes some poles cross the imaginary axis, which is the integration path. To preserve analyticity, the integration path must be deformed so that the crossing does not actually take place. Equivalently, we can keep the main integration path on the imaginary axis and add integration contours around the poles that have crossed the imaginary axis. In the end, we obtain a figure like


(2.8)

where the thick poles are the moving ones. When we make the Wick rotation to the real

(2.9)

(2.10)

A puzzling situation occurs when the right (respectively, left) LW pair of the propagator  $D(k^2, m_1^2, \epsilon_1)$  hits the left (right) LW pair of  $D((k-p)^2, m_2^2, \epsilon_2)$ , because in that case the integration path gets pinched. We call this occurrence *LW pinching*. The integration paths before and after the LW pinching are illustrated in the two pictures (2.9) and (2.10).

We show that, with these caveats, the procedure to handle the LW pinching is intrinsic to our definition of the theory, pretty much like the  $i\epsilon$  prescription is intrinsic to the definition of a theory as a Wick rotated Euclidean one. Moreover, it is consistent with perturbative unitarity.

The LW pinching motivated some authors to propose *ad hoc* prescriptions to handle it. The CLOP prescription [3], for example, amounts to deform the scale  $M$  in one of the propagators of the integral (2.6) to a different value  $M'$ . Under certain conditions, the pinching is absent for  $M' \neq M$  and the regions we mentioned above are analytically connected. In that situation, the Wick rotation is analytic everywhere. After the calculation of the amplitude, the deformed scale  $M'$  is sent to  $M$ . This operation cuts the complex plane into disconnected regions.

The CLOP prescription is not sufficient to deal with the LW pinching in all the diagrams, because higher-order diagrams are ambiguous, as shown in ref. [3]. Moreover, it appears to be artificial. For example, there is no obvious way to incorporate it into the Lagrangian or the Feynman rules. In this paper, we also show that the CLOP prescription leads to physical predictions that differ from the ones we obtain. We also show that, if we strictly apply the rules that follow from the formulation of this paper, it is possible to retrieve the correct result even starting from  $M' \neq M$  and letting  $M'$  tend to  $M$  at the end. Then, however, the CLOP prescription becomes redundant.

To summarize, we show that the theory is intrinsically equipped with the procedure that allows us to handle the LW pinching. The amplitudes are well defined and unambiguous. The prescriptions that can be found in the existing literature are either redundant or give predictions that are in contradiction with ours.

In section 6 we explain how the results of this section extend from the bubble diagram to more complicated diagrams.

### 3 LW pinching

In this section we describe the LW pinching in the case of the bubble diagram (2.5), that is to say the loop integral (2.6). First, we integrate on the loop energy  $k^0$  by means of the residue theorem along the imaginary axis. This operation leaves us with the integral on the loop space momentum  $\mathbf{k}$ . Orienting the external space momentum  $\mathbf{p}$  along the vertical line, the integral on the azimuth is trivial, so we remain with the integral on  $k_s \equiv |\mathbf{k}|$  from 0 to  $\infty$  and the integral on  $u \equiv \cos \theta$  from  $-1$  to  $1$ , where  $\theta$  is the zenith angle. To illustrate the problematics involved in the LW pinching exhaustively, we consider two cases. In the first case we work at  $\mathbf{p} = 0$ , in the second case we work at  $\mathbf{p} \neq 0$ . Lorentz invariance suggests that there should be no big difference between the two situations. It turns out that it is not so, because the method of calculation we are using is not manifestly Lorentz invariant. The calculation at  $\mathbf{p} = 0$  is equivalent to the one of ref. [7], which is well suited to apply the CLOP prescription and gives a Lorentz invariant result. However,

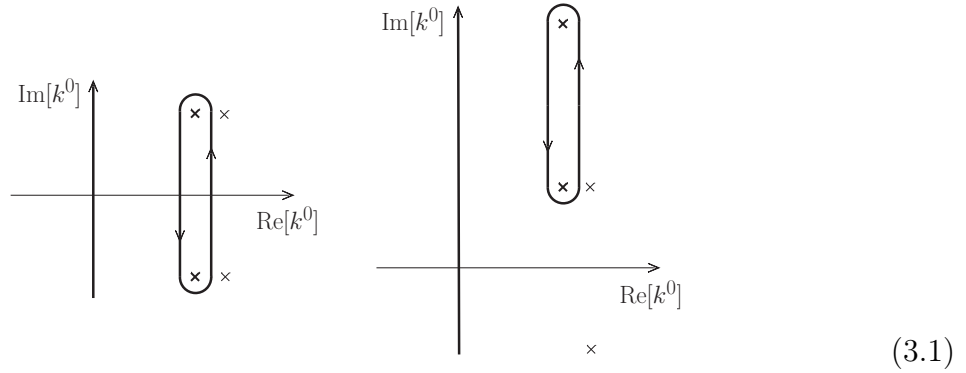


this approach misses a crucial point, which is visible only at  $\mathbf{p} \neq 0$ .

### 3.1 LW pinching at zero external space momentum

The LW pinching may involve pairs of LW poles (in which case it is called *pure* LW pinching) or one LW pole and a standard pole (in which case it is called *mixed* LW pinching). For the moment, we focus on the pure LW pinching, because at one loop the mixed one cannot occur for real external momenta.

There are two basic cases of pure LW pinching, shown in the figures



The first case involves the right LW pair of the first propagator and the left LW pair of the second propagator. The second case involves the upper-right LW pole of the first propagator and the bottom-left LW pole of the second propagator. The other LW pinchings are the complex conjugates of the ones just described and their reflections with respect to the imaginary axis.

At  $\mathbf{p} = 0$ , there is no  $u$  dependence, so the  $u$  integral is trivial, the only nontrivial integration variable being  $k_s$ . The poles relevant to the top pinching occurring in the left figure of (3.1) are

$$\frac{1}{k^0 - p^0 + \omega_M^*(\mathbf{k})} \frac{1}{k^0 - \omega_M(\mathbf{k})}, \quad (3.2)$$

while those relevant to the bottom pinching give the complex conjugate of this expression. The pinching occurs when  $k^0$  is such that the locations of the two poles coincide, which gives the pinching equation

$$p^0 = \sqrt{k_s^2 + iM^2} + \sqrt{k_s^2 - iM^2}, \quad (3.3)$$

solved by

$$k_s^2 = \frac{(p^0)^4 - 4M^4}{4(p^0)^2}. \quad (3.4)$$

The poles relevant to the pinching occurring in the right picture of (3.1) are

$$\frac{1}{k^0 - p^0 + \omega_M(\mathbf{k})} \frac{1}{k^0 - \omega_M(\mathbf{k})}.$$

They give the pinching equations

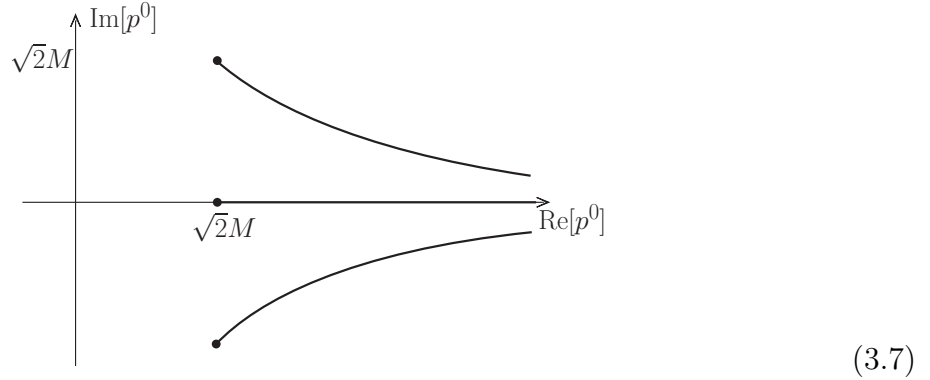
$$p^0 = 2\sqrt{k_s^2 + iM^2}, \quad (3.5)$$

which are solved by

$$k_s^2 = \frac{(p^0)^2}{4} - iM^2. \quad (3.6)$$

We denote the  $k_s$  integration path by  $\gamma_k$ . By default, we expect it to be the positive real axis. For the moment, we stick to this, but in a moment we will discover that we must deform  $\gamma_k$  to include complex values.

When  $k_s$  is real and positive, the solution of (3.3) exists for  $p^2$  real and larger than  $2M^2$ , while the solution of (3.5) exists when  $p^2 - 4iM^2$  is real and larger than zero. Performing the integral in  $\mathcal{J}(p)$ , we find the LW branch cuts shown in the picture



The middle branch point corresponds to the threshold  $p^2 = 2M^2$ , while the other two branch points correspond to the thresholds  $p^2 = 4iM^2$  and  $p^2 = -4iM^2$ . When we vary  $p^0$  across a branch cut of figure (3.7), a pole  $\nu$  of the  $k_s$  integrand crosses the  $k_s$  integration path  $\gamma_k$  (which means that the imaginary part of the pole becomes zero, while its real part stays positive), so the function  $\mathcal{J}(p)$  is not analytic in that point. We have not shown the branch cuts associated with the standard pinching and the mixed LW pinching.

For example, the right-hand side of (3.4) has vanishing imaginary part and positive real part for  $x \geq \sqrt{2}M$ ,  $y = 0$ , where  $x \equiv \text{Re}[p^0]$ ,  $y \equiv \text{Im}[p^0]$ . This gives the middle branch cut of figure (3.7), which starts from the branch point  $p^0 = \sqrt{2}M$ . A mirror branch cut is obtained by reflecting with respect to the imaginary axis.

On the other hand, the right-hand side of (3.6) has vanishing imaginary part and positive real part when

$$xy = 2M^2, \quad x^2 \geq y^2. \quad (3.8)$$

This gives the branch cut shown in the first quadrant of figure (3.7), which starts from the branch point  $p^0 = \sqrt{2}M(1 + i)$ , and a symmetric branch cut in the third quadrant. The complex conjugate LW pinching gives the branch cut shown in the fourth quadrant of figure (3.7), with branch point  $p^0 = \sqrt{2}M(1 - i)$ , and a symmetric branch cut in the second quadrant.

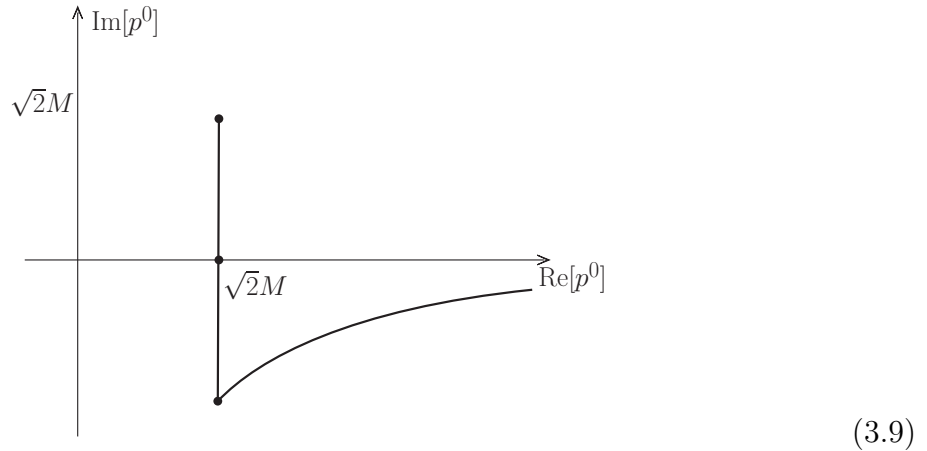
So far, we have described what happens when  $\gamma_k$  is kept rigid. We have seen that in that case certain poles  $\nu$  of the integrand cross  $\gamma_k$  when  $p^0$  crosses the cuts of figure (3.7). There, the function  $\mathcal{J}(p)$  is not analytic. This is what naturally happens if we make the integration numerically, since a generic integration program of numerical integration does not know how to analytically deform the integration paths.

If we want to turn  $\mathcal{J}(p)$  into a function that is analytic in a subdomain  $\mathcal{O}$  that intersects the branch cuts of figure (3.7), we have to move those branch cuts away from  $\mathcal{O}$ . This is done by deforming  $\gamma_k$  when the poles  $\nu$  approach it, so as to prevent  $\nu$  from crossing  $\gamma_k$  in  $\mathcal{O}$ , and make the crossing occur at different values of  $p^0$ . Equivalently, we can keep the integration path  $\gamma_k$  rigid, but add or subtract (depending on the direction of motion of  $\nu$ ) the residues of the moving poles  $\nu$  after the crossing. For example, in the equal mass case  $m_1 = m_2 = m$ , we can recover analyticity on the real axis above  $\sqrt{2}M$  by making the replacement

$$\mathcal{J}(p) \rightarrow \mathcal{J}(p) - \frac{1}{16\pi} \frac{M^4}{m^4 + M^4} \sqrt{1 - \frac{4M^4}{(p^2)^2}} \theta_-(p^2 - 2M^2),$$

when  $p^0$  crosses the real axis above  $\sqrt{2}M$  from the upper half plane in the first quadrant (from the lower half plane in the third quadrant), where  $\theta_-(x) = 1$  for  $\text{Re}[x] > 0$ ,  $\text{Im}[x] < 0$  and  $\theta_-(x) = 0$  in all other cases. In both sides of this replacement the integration path  $\gamma_k$  is the positive real axis.

Deforming the cuts with this procedure, we may obtain, for example, the picture



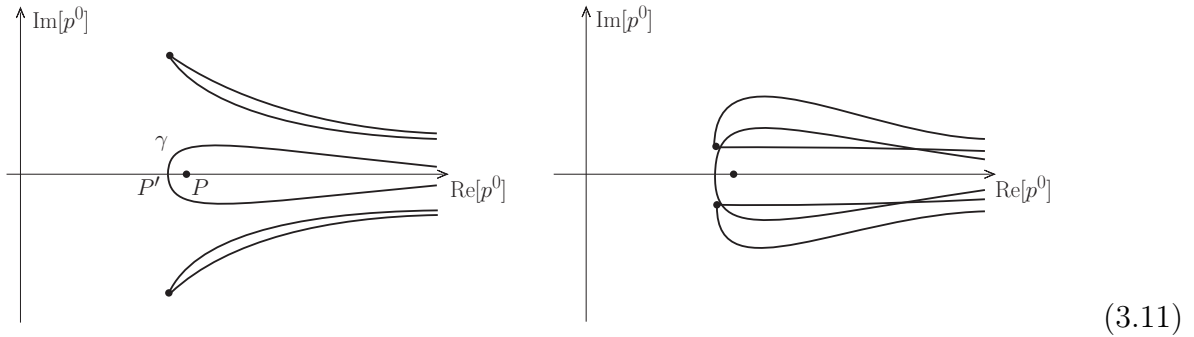
Now the amplitude is mathematically well defined on the real axis, but it has a nontrivial imaginary part for  $p^0$  real and such that  $(p^0)^2 > 2M^2$ , which violates unitarity. To preserve unitarity, we must keep the branch cuts symmetric with respect to the real axis. At  $\mathbf{p} = 0$  this implies that a branch cut is necessarily on the real axis, which makes the amplitude ill defined there.

### 3.2 LW pinching at nonzero external space momentum

At  $\mathbf{p} \neq 0$  several interesting phenomena occur, which eventually lead to the solution of the problem of properly handling the LW pinching. The pinching equations (3.3) and (3.5) become

$$p^0 = \sqrt{\mathbf{k}^2 + iM^2} + \sqrt{(\mathbf{k} - \mathbf{p})^2 - iM^2}, \quad p^0 = \sqrt{\mathbf{k}^2 + iM^2} + \sqrt{(\mathbf{k} - \mathbf{p})^2 + iM^2}, \quad (3.10)$$

respectively, plus their complex conjugates. Keeping  $\mathbf{p}$  fixed, we find the patterns



The first picture is obtained for smaller values of  $|\mathbf{p}|$ , the second picture for larger values. The interiors of the regions  $\tilde{\mathcal{A}}_i$  shown in these pictures are the values of  $p^0$  that satisfy the equations (3.10) for real  $\mathbf{k}$ . The cuts of (3.7) have enlarged into the regions  $\tilde{\mathcal{A}}_i$ , because the right-hand sides of (3.10) now depend on two parameters,  $k_s$  and  $u$ .

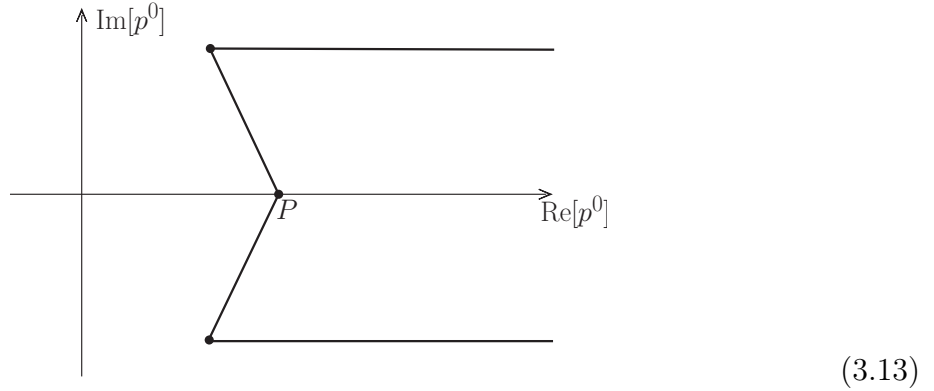
The point  $P$ , located at  $p^0 = \sqrt{2M^2 + \mathbf{p}^2} \equiv E_P$ , corresponds to the threshold  $p^2 = 2M^2$ . The curve  $\gamma$  is the boundary of the region  $\tilde{\mathcal{A}}_P$  that intersects the real axis. Note that  $\gamma$  does not cross the real axis in  $P$ , but in the point  $P'$ , which has energy

$$p^0 = \sqrt{\frac{\mathbf{p}^2}{2} + \sqrt{\frac{(\mathbf{p}^2)^2}{4} + 4M^4}} \equiv E_{P'} \quad (3.12)$$

and satisfies  $\sqrt{2}M < E_{P'} < E_P$ . Thus,  $\gamma$  can no longer be associated with a true branch cut. If we define the amplitude coherently with picture (3.11), Lorentz invariance is violated, because the intersection between  $\gamma$  and the real axis has no Lorentz invariant meaning. This fact has already been noticed by Nakanishi in ref. [6].

The intuitive reason behind the Lorentz violation is that, as shown in figure (2.4), the loop energy is not everywhere real. By Lorentz invariance, the loop momentum cannot be everywhere real. Thus, if we want to restore Lorentz invariance, we cannot keep the  $\mathbf{k}$  integration domain rigid. If we insist on keeping it rigid, Lorentz invariance is necessarily violated.

If we deform the  $\mathbf{k}$  domain of integration to complex values, we have several possibilities, but most of them violate unitarity, such as the deformation (3.9). To preserve unitarity, we must keep the picture symmetric with respect to the real axis. We deform the boundaries of the surfaces that appear in figure (3.11) into the branch cuts



plus other cuts symmetric to these ones with respect to the imaginary axis. In particular, the curve  $\gamma$  is deformed so as to maximize its distance from the origin. This means that it must cross the real axis in  $p^2 = 2M^2$ . The second thing to pay attention to is that the branch cuts must not cross the real axis anywhere else. This way, both Lorentz invariance and unitarity are preserved.

From the physical point of view, it does not really matter where the branch cuts of figure (3.13) are located, as long as they are symmetric with respect to the real axis and cross the real axis only in the threshold  $p^2 = 2M^2$ .

To summarize, at  $\mathbf{p} \neq 0$  the cuts of figure (3.7) and their reflections with respect to the imaginary axis are enlarged into regions  $\tilde{\mathcal{A}}_i$ . Lorentz invariance is violated, but can be restored by analytically deforming each region  $\tilde{\mathcal{A}}_i$  into a new region  $\mathcal{A}_i$ . The extension must be maximal “from below”, which means from smaller to larger values of  $p^2$ . In the end, the complex plane is divided into three disjoint analytic regions  $\mathcal{A}_i$ . The imaginary axis is fully contained in one of them, called *main analytic region*. The other two regions are symmetric with respect to the imaginary axis. The right region can be reached from the main region in a nonanalytic way, by crossing one of the branch cuts shown in (3.13), while keeping the  $\mathbf{k}$  domain of integration rigid.

By means of this construction, the amplitude is unambiguous, Lorentz invariant and

satisfies unitarity. Now it is clear why we say that the Lee-Wick models are formulated as nonanalytically Wick rotated Euclidean higher-derivative theories.

## 4 Calculation around the LW pinching

In this section we show that the amplitudes are well defined without the need of *ad hoc* prescriptions. Moreover, the nonanalyticity just occurs on the boundaries of the surfaces shown in figure (3.11), but not inside.

We focus on the pinching depicted in the left figure of (3.1). The  $\mathbf{k}$  integral has potential singularities of the form  $1/D_0$  and  $1/D_0^*$ , where

$$D_0 = p^0 - \omega_M(\mathbf{k}) - \omega_M^*(\mathbf{k} - \mathbf{p}). \quad (4.1)$$

The top pinching occurs for  $D_0 = 0$ , i.e.

$$p^0 = \sqrt{\mathbf{k}^2 + iM^2} + \sqrt{(\mathbf{k} - \mathbf{p})^2 - iM^2}, \quad (4.2)$$

while the bottom pinching occurs for  $D_0^* = 0$ . The crucial point of the argument that follows is that the condition is complex for  $\mathbf{p} \neq 0$  (while it becomes real at  $\mathbf{p} = 0$ ), so it splits into two real conditions.

Our goal is to calculate the physical amplitude above the threshold of the LW pinching, so we take a real  $p^0 > \sqrt{\mathbf{p}^2 + 2M^2}$ . Moreover, we take the loop space momentum  $\mathbf{k}$  real, since in this analytic region we can keep the  $\mathbf{k}$  integration path rigid. Then, the solution of (4.2) is a circle, equal to the intersection between a sphere and a plane, given by

$$\mathbf{k}^2 = \frac{(p^0)^4 - 4M^4}{4(p^0)^2}, \quad \mathbf{p}^2 = 2\mathbf{p} \cdot \mathbf{k}. \quad (4.3)$$

We can generalize the analysis to complex external energies  $p^0$ . The main arguments are the same, but the solutions become more involved. It is sufficient to extend the solution of (4.2) to the values of  $p^0$  that are closed to the real axis, by making the substitution  $p^0 \rightarrow p^0 e^{i\varphi}$ , with  $\varphi$  small. Then the denominator becomes

$$D_\varphi = p^0 e^{i\varphi} - \omega_M(\mathbf{k}) - \omega_M^*(\mathbf{k} - \mathbf{p}).$$

To simplify the formulas, we expand  $D_\varphi$  around the solution (4.3) by means of the change of variables

$$k_s = \frac{\sigma_-}{2p^0} + \tau \frac{\sigma_+^2}{2\sigma_- (p^0)^2} + \eta \frac{p_s \sigma_+^2}{4\sigma_- M^2}, \quad u = \frac{p_s}{2k_s} + \eta \frac{\sigma_+^2}{2\sigma_- M^2}, \quad (4.4)$$

where  $\sigma_{\pm} \equiv \sqrt{(p^0)^4 \pm 4M^4}$ ,  $p_s \equiv |\mathbf{p}|$  and  $u = \cos \theta$ ,  $\theta$  being the angle between the vectors  $\mathbf{p}$  and  $\mathbf{k}$ . The fluctuations around the singular loci (4.3) are parametrized by  $\tau$  and  $\eta$ . The parametrization (4.4) is chosen to simplify the behavior of the  $\mathbf{k}$  integral around the solution. The integrand is proportional to

$$\frac{d^{D-1}\mathbf{k}}{D_{\varphi}} \rightarrow -\frac{2\pi^{(D-2)/2}}{\Gamma\left(\frac{D}{2}-1\right)} \frac{k_s^{D-2} dk_s (1-u^2)^{(D-4)/2} du}{\tau - i(p^0\varphi + p_s\eta)}, \quad (4.5)$$

where the arrow means that we integrate on all the angles besides  $\theta$ . We have expanded the denominator to the first order in  $\varphi$ .

We see that the integral is regular as long as either  $\varphi$  or  $p_s$  are different from zero, which means that in those cases the potential singularity at  $D_0 = 0$  is integrable. If we keep  $p_s \neq 0$  and reach  $\varphi = 0$ , we obtain

$$\frac{d^{D-1}\mathbf{k}}{D_0} = -\frac{2\pi^{(D-2)/2}}{\Gamma\left(\frac{D}{2}-1\right)} \frac{\sigma_+^4 [\sigma_-^2 - (p^0)^2 p_s^2]^{(D-4)/2}}{(2p^0)^D M^2} \frac{d\tau d\eta}{\tau - ip_s\eta}. \quad (4.6)$$

It is interesting to study the limit  $p_s \rightarrow 0$ , which gives

$$-\frac{2\pi^{(D-2)/2}}{\Gamma\left(\frac{D}{2}-1\right)} \frac{\sigma_+^4 \sigma_-^{D-4}}{(2p^0)^D M^2} d\tau d\eta \left[ \mathcal{P}\left(\frac{1}{\tau}\right) + i\pi \text{sgn}(\eta) \delta(\tau) \right], \quad (4.7)$$

where  $\mathcal{P}$  denotes the principal value and  $\text{sgn}$  is the sign function. We learn that, basically,  $p_s$  provides the prescription for handling the integral. Note that at  $p_s = 0$  no  $\eta$  dependence survives in the integrand, besides the sign function of formula (4.7). If we perform the trivial  $\eta$  integration, we finally get

$$-\frac{8\pi^{(D-2)/2}}{\Gamma\left(\frac{D}{2}-1\right)} \frac{\sigma_+^2 \sigma_-^{D-3}}{(2p^0)^D} d\tau \mathcal{P}\left(\frac{1}{\tau}\right). \quad (4.8)$$

In three and higher dimensions there is no singularity for  $\sigma_- \rightarrow 0^+$ .

To illustrate the procedure better, we check what happens when we pursue a different strategy (which turns out to be unacceptable), by first setting  $p_s = 0$  at nonzero  $\varphi$  and then send  $\varphi$  to zero. To this purpose, it is sufficient to replace the denominator  $\tau - ip_s\eta$  of formula (4.6) with  $\tau - ip^0\varphi$ . After integrating on  $\eta$ , we find

$$-\frac{8\pi^{(D-2)/2}}{\Gamma\left(\frac{D}{2}-1\right)} \frac{\sigma_+^2 \sigma_-^{D-3}}{(2p^0)^D} \frac{d\tau}{\tau - ip^0\varphi} \xrightarrow{\varphi \rightarrow 0^{\pm}} -\frac{8\pi^{(D-2)/2}}{\Gamma\left(\frac{D}{2}-1\right)} \frac{\sigma_+^2 \sigma_-^{D-3}}{(2p^0)^D} d\tau \left[ \mathcal{P}\left(\frac{1}{\tau}\right) \pm i\pi \delta(\tau) \right]. \quad (4.9)$$

This expression is also regular, but does not coincide with (4.8).

Formula (4.8) is certainly correct, because it is obtained by approaching the real axis from  $p_s \neq 0$ , where the region  $\tilde{\mathcal{A}}_P$  contains a neighborhood of the real axis above the

threshold  $p^2 = 2M^2$ . Instead, (4.9) is obtained by first squeezing the region  $\tilde{\mathcal{A}}_P$  to the real axis (which is a consequence of letting  $p_s \rightarrow 0$  first) and then approaching the real axis from the complex plane. Thus, (4.9) cannot be correct.

We learn that the theory knows how to deal with the LW pinching unambiguously. Moreover, the nonanalytic Wick rotation does work, is free of singularities and consistent with unitarity. In section 5 we complete the calculation of the bubble diagram.

## 4.1 Comparison with the CLOP and other prescriptions

We have seen that the theory is intrinsically equipped with the right recipe to handle the LW pinching, which is (4.8). This means that any artificial prescription can potentially lead to wrong results. Now we classify the whole set of unitary prescriptions, which includes the CLOP one, and compare them with the results predicted by the formulation of this paper. For definiteness, we work in four dimensions.

Consider the integrand of the loop integral (2.6) at  $\mathbf{p} = 0$ . We begin with the top pinching that appears in the left figure of (3.1), which is due to the poles (3.2). By means of the expansion

$$k_s = \frac{\sigma_-}{2p^0} + \tau \frac{Mp^0}{\sigma_-}, \quad (4.10)$$

we see that the integrand of  $\mathcal{J}(p)$  behaves as

$$\frac{i}{(8\pi)^2} \frac{\sigma_-}{(p^0)^2} \frac{M^4}{(M^2 + im_1^2)(M^2 - im_2^2)} \frac{d\tau}{\tau} \quad (4.11)$$

around the singularity  $\tau = 0$ .

We know that the formulation of this paper removes the singularity because, working at nonvanishing  $\mathbf{p}$  and letting  $\mathbf{p}$  tend to zero afterwards, (4.11) is replaced by

$$\frac{i}{(8\pi)^2} \frac{\sigma_-}{(p^0)^2} \frac{M^4}{(M^2 + im_1^2)(M^2 - im_2^2)} \mathcal{P} \left( \frac{1}{\tau} \right) d\tau.$$

More generally, we may have

$$\frac{i}{(8\pi)^2} \frac{\sigma_-}{(p^0)^2} \frac{M^4}{(M^2 + im_1^2)(M^2 - im_2^2)} \left[ \mathcal{P} \left( \frac{1}{\tau} \right) + ia\delta(\tau) \right] d\tau, \quad (4.12)$$

where  $a$  is an arbitrary real constant.

The LW poles come in conjugate pairs, so the pinching just considered is accompanied by the complex conjugate one, which occurs when the residue calculated in  $k^0 = p^0 - \omega_M(\mathbf{k})$  hits the LW pole located in  $k^0 = \omega_M^*(\mathbf{k})$ . The contribution is minus the complex conjugate



of (4.12), because the  $i$  factor that accompanies the residue does not get conjugated. The total gives

$$\frac{2i}{(8\pi)^2} \frac{\sigma_-}{(p^0)^2} \frac{M^4}{(M^4 + m_1^4)(M^4 + m_2^4)} \left[ (M^4 + m_1^2 m_2^2) \mathcal{P}\left(\frac{1}{\tau}\right) + a M^2 (m_1^2 - m_2^2) \delta(\tau) \right] d\tau.$$

We see that the contribution to the amplitude is regular and purely imaginary. In particular, it does not affect the cutting equations, which concern the sum of  $\mathcal{J}(p)$  plus its conjugate. This result proves that the prescription (4.12) is consistent with perturbative unitarity for arbitrary  $a$ . However, the loop integral  $\mathcal{J}(p)$  does depend on  $a$ , at least when the two masses are different. This proves that no prescription with nonvanishing  $a$  is consistent with our formulation, which predicts  $a = 0$ .

In particular, the CLOP prescription gives  $a = \pm\pi$ . This result can be proved by replacing the LW scale  $M$  with  $M' = M + \delta$  in the second propagator of (2.6). Modifying the expansion (4.10) into

$$k_s = \frac{\sigma_-}{2p^0} + \tau \frac{M p^0}{\sigma_-} - 2\delta \frac{M^3}{p^0 \sigma_-},$$

the integrand  $\mathcal{J}(p)$  behaves as

$$\frac{i}{(8\pi)^2} \frac{\sigma_-}{(p^0)^2} \frac{i M^4}{(M^2 + i m_1^2)(M^2 - i m_2^2)} \frac{d\tau}{\tau - i\delta},$$

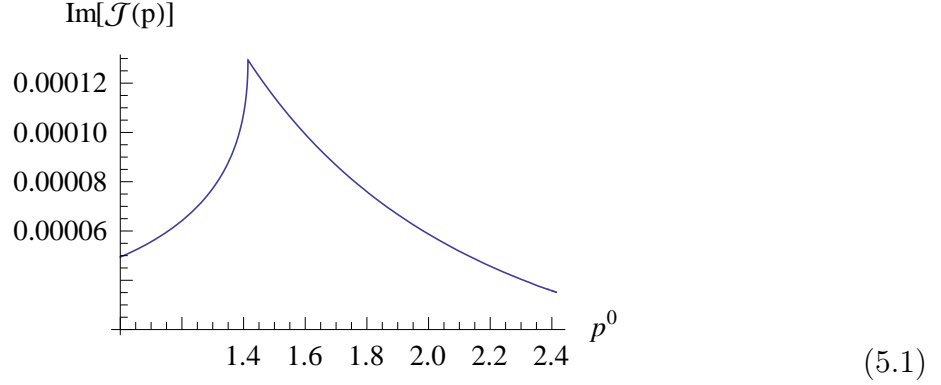
around the top pinching of the left figure of (3.1). This formula is equivalent to (4.12) with  $a = \pi \text{sgn}(M' - M)$ . Thus, the CLOP prescription should be dropped, because it is not consistent with our formulation.

## 5 Complete bubble diagram

In this section, we complete the calculation of the bubble diagram. The main goal is to describe what happens around the LW threshold. The threshold associated with the physical poles is not the main focus of the calculation, so, to avoid the superposition between the physical threshold and the LW one, we assume that the mass  $m$  is sufficiently large. For concreteness, we take  $m = 3M$ .

Another simplifying choice is to make the calculation at  $\mathbf{p} = 0$  and resolve the singularity with the help of formula (4.8). We know that this procedure is justified by starting from nonvanishing  $\mathbf{p}$ , where the LW pinching is properly handled, and taking the limit  $\mathbf{p} \rightarrow 0$  afterwards.

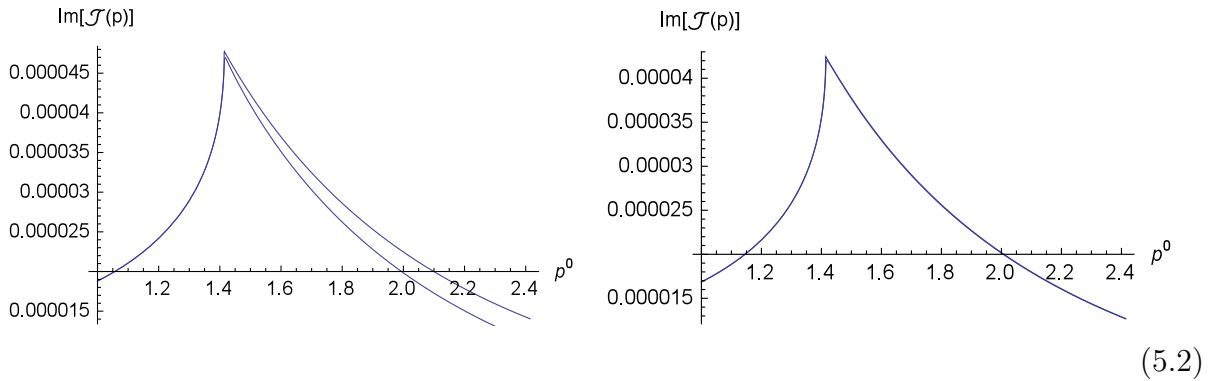
Setting  $M = 1$ , the imaginary part of  $\mathcal{J}(p)$  as a function of a real  $p^0$  has the behavior



while the real part vanishes, which confirms unitarity. We see that the imaginary part is well defined and continuous, but not analytic. The nonanalyticity that is visible at  $p^2 = 2M^2$  is the remnant of the LW pinching. If in nature some physical processes are described by a LW theory, the LW scale  $M$  is the key physical quantity signaling the new physics. A shape like (5.1) may be helpful to determine the magnitude of  $M$  experimentally.

We stress again that the nonanalytically Wick rotated Euclidean theory does not need a particular prescription. Because of this, we expect that it also eliminates the ambiguities that the CLOP prescription is claimed to generate in more complicated diagrams [3].

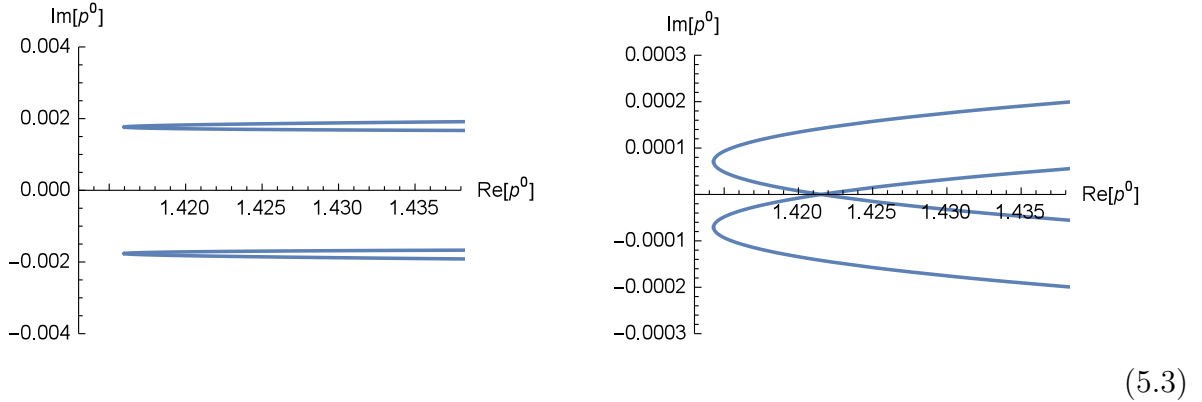
The CLOP prescription gives the same result, in the case just considered. As explained in the previous section, we can appreciate the difference between the predictions of our formulation and those of the CLOP prescription in the bubble diagram with unequal masses. For example, we compare the cases  $m_1 = 3$ ,  $m_2 = 5$  and  $m_1 = m_2 = 4$ . Using the CLOP prescription, we take  $M = 1$  in the first propagator of formula (2.6) and  $M = 1 + \delta$  in the second propagator, working at  $\mathbf{p} = 0$ . Then we integrate  $\mathcal{J}(p)$  numerically for smaller and smaller values of  $\delta$ , till, say,  $\delta = 10^{-3}$ . On the other hand, following the formulation proposed here, we set  $M = 1$  in both propagators, but keep  $p_s = |\mathbf{p}|$  different from zero. Then, we integrate numerically for smaller and smaller values of  $p_s$  till  $p_s = 10^{-3}$ . The imaginary part of  $\mathcal{J}(p)$  gives the pictures



while the real part still vanishes. The first figure refers to the case  $m_1 = 3$ ,  $m_2 = 5$ , while the second figure refers to the case  $m_1 = m_2 = 4$ . The upper graph is the one predicted by our formulation, while the lower graph is the one coming from the CLOP prescription. The match is very precise in the equal mass case, but there is a remarkable discrepancy above the LW threshold in the unequal mass case. The result confirms that the CLOP prescription is not compatible with the formulation proposed here.

If we really want to retrieve our result from a procedure where the propagators of formula (2.6) have two different LW scales  $M$  and  $M'$ , as in the CLOP prescription, we actually can, but in that case the CLOP prescription becomes redundant. Instead of setting  $p_s = 0$  and then letting  $M'$  tend to  $M$ , we must start from  $p_s \neq 0$ , let  $M'$  approach  $M$  while  $p_s \neq 0$ , work in a suitable region  $\tilde{\mathcal{A}}_>$ , analytically continue “from above” and only at the end, if we want, let  $p_s$  tend to zero.

The region  $\tilde{\mathcal{A}}_P$  contained in the curve  $\gamma$  of the first figure shown in (3.11) splits into two regions  $\tilde{\mathcal{A}}_P^+$  and  $\tilde{\mathcal{A}}_P^-$ , when  $M' = 1 + \delta$  is sufficiently different from  $M$  (or  $p_s$  sufficiently large):



In both figures, we have  $p_s = 10^{-3}$  and  $M = 1$ . In the first figure  $\delta = 5 \cdot 10^{-3}$ , while in the second figure  $\delta = 10^{-4}$ .

We see that when  $\delta$  is sufficiently large the real axis has no intersection with  $\tilde{\mathcal{A}}_P^+$  and  $\tilde{\mathcal{A}}_P^-$ . Instead, when  $\delta$  becomes smaller, the region  $\tilde{\mathcal{A}}_> \equiv \tilde{\mathcal{A}}_P^+ \cap \tilde{\mathcal{A}}_P^-$  is nonempty. What the CLOP prescription requires is to cover the entire real axis by analytic continuation from below (i.e. from the region that contains the imaginary axis) and let  $\delta$  tend to zero at the end. What our formulation requires, instead, is to cover the portion of the real axis that is located above the LW threshold by analytic continuation from above, i.e. from  $\tilde{\mathcal{A}}_>$ . This is the crucial difference between the two formulations, which explains the discrepancy shown in figure (5.2).

## 6 More complicated diagrams

The arguments of the previous sections extend to more complicated diagrams, but some remarks on how to deal with them are in order. In the one-loop diagrams, the loop momentum remains unique, while the independent external momenta become more than one. The mixed LW pinching cannot occur for real external momenta. On the other hand, figure (2.10) shows that the pure LW pinchings are entirely similar to the ones of the bubble and occur between the right LW poles of any propagator and the left LW poles of any other propagator.

At higher loops the pinching is not so different from the one we are accustomed to in standard theories. There, if the propagators of the internal legs of the diagram have masses  $m_i$ , the pinchings lead to thresholds of the form  $p^2 = (m_{i_1} + m_{i_2} + m_{i_3} + \dots)^2$ , where  $p$  is a linear combination of incoming momenta. In the case of the LW pinching, the formulas that give the thresholds are basically the same, with the difference that some masses  $m_i$  may be replaced by the complex masses  $M_{\pm} = (1 \pm i)M/\sqrt{2}$  associated with the LW scales. We get the thresholds

$$p^2 = \left[ (n_+ + n_-) \frac{M}{\sqrt{2}} + i(n_+ - n_-) \frac{M}{\sqrt{2}} + m_{i_1} + m_{i_2} + m_{i_3} + \dots \right]^2,$$

where the integers  $n_+$  and  $n_-$  are the numbers of masses  $M_+$  and  $M_-$ , respectively. The number of thresholds grows with the number of loops and so does the number of disjoint analytic regions  $\mathcal{A}_i$ . The thresholds that are relevant to the calculations of the physical amplitudes are those that are located on the real axis, which are

$$p^2 = (\sqrt{2}nM + m_{i_1} + m_{i_2} + m_{i_3} + \dots)^2,$$

where  $n = n_+ = n_-$ .

The analytic regions  $\mathcal{A}_i$  are determined as follows. Working in a generic Lorentz frame, we find the regions  $\tilde{\mathcal{A}}_i$  by keeping the integrations on the loop space momenta rigid everywhere [see (3.11)]. Then, we maximally extend each  $\tilde{\mathcal{A}}_i$  “from below”, which means from smaller to larger values of the squared external momenta  $p^2$ , till we reach a threshold [see (3.13)], where we must stop. Once the regions  $\mathcal{A}_i$  are known we restrict the calculation of the loop integral to subsets  $\mathcal{O}_i \subset \tilde{\mathcal{A}}_i$  that contain at least one accumulation point, where we can keep the integral on the space momenta rigid. Then we analytically continue the result to  $\mathcal{A}_i$ .

## 7 Conclusions

The Lee-Wick models are higher-derivative theories that are claimed to reconcile renormalizability and unitarity in a very nontrivial way. However, several aspects of their formulation have remained unclear, so far. In this paper, we have provided a new formulation of the models that overcomes the major difficulties, by defining them as nonanalytically Wick rotated Euclidean theories. Working in a generic Lorentz frame, the models are intrinsically equipped with the right recipe to treat the pinchings of the Lee-Wick poles, with no need of external *ad hoc* prescriptions. The complex energy plane is divided into disconnected analytic regions, which are related to one another by keeping the integration path on the space momentum rigid when certain poles cross it.

The physical results that follow from our approach are quantitatively different from those of the previous approaches. The nonanalytic behaviors of the amplitudes may have interesting phenomenological consequences, which may facilitate the measurements of some key physical constants of the theories, such as the scales associated with the higher-derivative terms.

## Acknowledgments

We are grateful to U.G. Aglietti and L. Bracci for useful discussions.

## References

- [1] T.D. Lee and G.C. Wick, Negative metric and the unitarity of the S-matrix, Nucl. Phys. B 9 (1969) 209.
- [2] T.D. Lee and G.C. Wick, Finite theory of quantum electrodynamics, Phys. Rev. D 2 (1970) 1033.
- [3] R.E. Cutkosky, P.V. Landshoff, D.I. Olive, and J.C. Polkinghorne, A non-analytic S-matrix, Nucl. Phys. B 12 (1969) 281.
- [4] K.S. Stelle, Renormalization of higher derivative quantum gravity, Phys. Rev. D 16 (1977) 953;  
E. S. Fradkin and A. A. Tseytlin, Renormalizable asymptotically free quantum theory of gravity, Nucl. Phys. B 201 (1982) 469.

- [5] U.G. Aglietti and D. Anselmi, Inconsistency of Minkowski higher-derivative theories, Eur. Phys. J. C 77 (2017) 84, 16A2 Renormalization.com and arXiv:1612.06510 [hep-th].
- [6] N. Nakanishi, Lorentz noninvariance of the complex-ghost relativistic field theory, Phys. Rev. D 3, 811 (1971).
- [7] B. Grinstein, D. O’Connell and M.B. Wise, Causality as an emergent macroscopic phenomenon: The Lee-Wick  $O(N)$  model, Phys. Rev. D 79 (2009) 105019 and arXiv:0805.2156 [hep-th].
- [8] B. Grinstein, D. O’Connell, and M.B. Wise, The Lee-Wick standard model, Phys. Rev. D 77 (2008) 025012 and arXiv:0704.1845 [hep-ph];  
C.D. Carone and R.F. Lebed, Minimal Lee-Wick extension of the standard model, Phys. Lett. B 668 (2008) 221 and arXiv:0806.4555 [hep-ph];  
J.R. Espinosa and B. Grinstein, Ultraviolet properties of the Higgs sector in the Lee-Wick standard model, Phys. Rev. D 83 (2011) 075019 and arXiv:1101.5538 [hep-ph];  
C.D. Carone and R.F. Lebed, A higher-derivative Lee-Wick standard model, JHEP 0901 (2009) 043 and arXiv:0811.4150 [hep-ph].
- [9] B. Grinstein and D. O’Connell, One-Loop Renormalization of Lee-Wick Gauge Theory, Phys. Rev. D 78 (2008) 105005 and arXiv:0801.4034 [hep-ph];  
C. D. Carone, Higher-derivative Lee-Wick unification, Phys. Lett. B 677 (2009) 306, and arXiv:0904.2359 [hep-ph].
- [10] E. Tomboulis,  $1/N$  expansion and renormalization in quantum gravity, Phys. Lett. B 70 (1977) 361;  
E. Tomboulis, Renormalizability and asymptotic freedom in quantum gravity, Phys. Lett. B 97 (1980) 77;  
Shapiro and L. Modesto, Superrenormalizable quantum gravity with complex ghosts, Phys. Lett. B 755 (2016) 279-284 and arXiv:1512.07600 [hep-th];  
L. Modesto, Super-renormalizable or finite Lee-Wick quantum gravity, Nucl. Phys. B 909 (2016) 584 and arXiv:1602.02421 [hep-th].